State estimation in wall-bounded flow systems. Part 2. Turbulent flows

By MATTIAS CHEVALIER[1,2], JÉRÔME HŒPFFNER[2], THOMAS R. BEWLEY[3] AND DAN S. HENNINGSON[1,2]

[1]The Swedish Defense Research Agency (FOI), SE-172 90, Stockholm, Sweden

[2]Department of Mechanics, Royal Institute of Technology, S-100 44, Stockholm, Sweden

[3]Department of Mechanical and Aerospace Engineering, University of California San Diego, La Jolla, CA 92093, USA

(Received 12 January 2005)

This work extends the estimator developed in Part 1 of this study (Hœpffner et al., *J. Fluid Mech.*, submitted) to the problem of estimating a turbulent channel flow at $Re_\tau = 100$ based on a history of noisy measurements on the wall. The key advancement enabling this work is the development and implementation of an efficient technique to extract, from direct numerical simulations, the relevant statistics (mean and covariance) of an appropriately-defined "external forcing" term on the Navier–Stokes equation linearized about the mean turbulent flow profile. This forcing term is designed to account for the unmodelled (nonlinear) terms during the computation of the (linear) Kalman filter feedback gains at each wavenumber pair $\{k_x, k_z\}$. The statistics of this forcing term are found to have some similarities to the parameterization of the external disturbances considered in Part 1 of this study, which dealt with the estimation of the early stages of transition in the same domain. Three key steps were identified in obtaining adequate estimator performance in the near-wall region: 1) linearization the flow system about the mean turbulent flow profile, accounting for the statistics of the additional forcing term during the computation of the feedback gains, 2) extraction of these statistics from a direct numerical simulation, and 3) incorporation of the nonlinearity of the actual system into the estimator model at the final step in the development of the estimator (using an extended Kalman filter). Upon inverse transform of the resulting feedback gains computed on an array of wavenumber pairs, we obtain, as in Part 1, effective and well-resolved feedback convolution kernels for the estimation problem.

It is demonstrated that by applying the optimal feedback gains, for all three measurements, satisfactory correlation between the actual and estimated flow is obtained in the near-wall regions. The correlation eventually decays as the wall distance increases but the decay sets in later compared to using estimation gains based on a statistically uncorrelated stochastic models. Both Kalman and extended Kalman filters are evaluated and naturally the extended filter is giving better correlations between the actual and estimated flow, however the Kalman filter gives good performance in the near-wall regions.

---

1. Introduction

This paper builds directly on Part 1 of this study (Hœpffner et al., *J. Fluid Mech.*, submitted, hereafter referred to as Part 1). It extends the estimator developed there, for the case of perturbed laminar channel flow, to the problem of fully-developed channel-flow turbulence. The reader is referred to Part 1 for related general references, background information on optimal state estimation (Kalman filter) theory, and a description of what it takes to apply this theory to a well-resolved discretization of a fluid system in a manner that is consistent with the continuous PDE system upon which this discretization is based (that is, in a manner such that the resulting feedback convolution kernels converge upon refinement of the numerical grid). The present paper effectively picks up where Part 1 left off, and treats specifically the issues involved in extending the estimator developed in Part 1 to the problem of estimating a fully-developed turbulent channel flow based on wall measurements.

1.1. *Model predictive estimation*

There are two natural approaches for model-based estimation of near-wall turbulent flows: model predictive estimation and extended Kalman filtering. Bewley & Protas (2004) discusses the model predictive estimation approach, which is based on iterative state and adjoint calculations, optimizing the estimate of the state of the system such that the nonlinear evolution of the system model, over a finite horizon in time, matches the available measurements to the maximum extent possible. This is typically accomplished by optimizing the initial conditions in the estimator model in order to minimize a cost function measuring a mean-square "misfit" of the measurements from the corresponding quantities in the estimator model over the time horizon of interest. This optimization is performed iteratively, using gradient information provided by calculation of an appropriately-defined adjoint field driven by the measurement misfits at the wall. The technique provides an optimized estimate of the state of the system which accounts for the full nonlinear evolution of the system, albeit over a finite time horizon and providing only a local optimal which might be far from the actual flow state sought. The technique is typically expensive computationally, as it requires iterative marches of the state and adjoint fields over the time horizon of interest in order to obtain the state estimate; for this reason, this approach is often quickly disqualified from consideration as being computationally intractable for practical implementation. The model predictive estimation approach is closely related to the adjoint-based approach to weather forecasting, commonly known as 4D-var. For further discussion of model predictive estimation as it applies to near-wall turbulence, the reader is referred to Bewley & Protas (2004).

1.2. *Extended Kalman filtering*

The extended Kalman filter approach, which is the focus of the present paper, is described in detail in Part 1 of this study. To summarize it briefly, the estimation problem is first considered in the linearized setting. Define $\hat{r}_m$ as the Fourier transform of the vector of all three measurements available on the walls in the actual flow system at wavenumber pair $\{k_x, k_z\}$, and define $\hat{r}$ as the corresponding quantity in the estimator model. At each wavenumber pair $\{k_x, k_z\}$, a set of feedback gains L is first computed such that a forcing term $\hat{v} = L(\hat{r}_m - \hat{r})$ on the (linearized) estimator model results in a minimization of the energy of the estimation error (that is, this feedback minimizes the trace of the covariance of the estimation error, usually denoted P), assuming the flow state itself is also governed by the same linearized model. This is called a Kalman filter, and the theory for the calculation of the optimal feedback gain L in the estimator is elegant, mathematically rigorous, and well known†.

Upon inverse transform of the resulting feedback gains computed on an array of

† For a succinct introduction in the spatially-discrete (ODE) setting, see, e.g., p. 463–470 of Lewis & Syrmos (1995). For a more comprehensive presentation in the ODE setting, see

wavenumber pairs, we seek (and, indeed, find) well resolved feedback convolution kernels for the estimation problem that, far enough from the origin (that is, from , decay exponentially with distance from the origin. The reader is referred to Bamieh (1997), Bewley (2001) and Högberg *et al.* (2003*a*) for further discussion of

(*a*) the technique used to transform feedback gains in Fourier space to feedback convolution kernels in physical space,

(*b*) interpretation of what these convolution kernels mean in both the control and estimation problems, and

(*c*) description of the overlapping decentralized control implementation facilitated by this approach, which is built from an interconnected array of identical tiles, each with actuators, sensors, and control logic incorporated, that communicate only with their neighbors.

Ultimately, the estimator feedback $\hat{v} = L(\hat{r}_m - \hat{r})$ is applied to a full (nonlinear) model of the flow system. This final step of reintroducing the nonlinearity of the system into the estimator model results in what is called an extended Kalman filter. In practice, the extended Kalman filter has proved to be one of the most reliable techniques available for estimating the evolution of nonlinear systems.

1.3. *On the suitability of linear models of turbulence for state estimation and control*

As described in the previous section, the feedback kernels used in the extended Kalman filter are calculated based on a linearized model of the fluid system. Thus, the applicability of the extended Kalman filtering strategy to turbulence is predicated upon the hypothesis that linearized models faithfully represent at least some of the important dynamic processes in turbulent flow systems.

The fluid dynamics literature of the last decade is replete with articles aimed at supporting this hypothesis. For example, Farrell & Ioannou (1996) used these linearized equations in an attempt to explain the mechanism for the turbulence attenuation that is caused by the closed-loop control strategy now commonly known as opposition control. Jovanović & Bamieh (2001) proposed a stochastic disturbance model which, when used to force the linearized open-loop Navier–Stokes equation, led to a simulated flow state with certain second-order statistics (specifically, u_{rms}, v_{rms}, w_{rms}, and the Reynolds stress $-\overline{uv}$) that mimicked, with varying degrees of precision, the statistics from a full DNS of a turbulent flow at $Re_\tau = 180$.

Clearly, however, the hypothesis concerning the relevance of linearized models to the turbulence problem can only be taken so far, as linear models of fluid systems do not capture the nonlinear "scattering" or "cascade" of energy over a range of length scales and time scales, and thus linear models fail to capture an essential dynamical effect that endows turbulence with its inherent "multiscale" characteristics. The key philosophy of the present work (and, indeed, the key philosophy motivating our application of linear control theory to turbulence in general), is that the fidelity required of a model for it to be adequate for control (or estimator) design is in fact much lower than the fidelity required of a model for it to be adequate for accurate simulation of the system. Thus, for the purpose of computing feedback for the control and estimation problems, linear models might well be good enough, even though the fidelity of linear models as simulation tools to capture the open-loop statistics of turbulent flows is still the matter of some debate in the fluids literature. All that the feedback in an extended Kalman filter has to do is to give the estimator model a "nudge" in approximately the right direction when the

Anderson & Moore (1979). For the corresponding derivation in the spatially-continuous (PDE) setting, see Balakrishnan (1976).

state and the state estimate are diverging. The extended Kalman filter contains the full nonlinear equations of the actual system in the estimator model, so if the state and the state estimate are sufficiently close, the estimator will accurately track the state, for at least a short period of time, with little or no additional forcing necessary.

Stating this philosophy another way, in the control problem, the model upon which the control feedback is computed need only include the key terms responsible for the production of energy. Since the nonlinear terms in the Navier–Stokes equations are conservative, and thereby do not contribute directly to energy production, we can expect that a linear model may suffice. For Navier–Stokes systems near solid walls, there is evidence that this is in fact true, at least for sufficiently low Reynolds number. Kim & Lim (2000) showed that interior body forcing (applied everywhere inside the flow domain) that was constructed to exactly cancel the linear coupling term in the linear part of the nonlinear Navier–Stokes equation (that is, canceling the $\mathcal{L}_C$ term in (2.4)) was sufficient to completely relaminarize the turbulent flow. Högberg *et al.* (2003*b*) showed that blowing and suction distributed on the channel walls that was determined using full-information linear control theory (scheduling the feedback gains based on the instantaneous shape of the mean velocity profile) was also sufficient to completely relaminarize the turbulent flow.

The present work on the estimation problem is based on the related philosophy that, in a similar manner, the model upon which the estimator feedback is computed need only capture the key terms responsible for the production of energy in the system describing the estimation error.

1.4. *The problem of nearly unobservable modes*

The problem of estimating the state of a chaotic nonlinear system based on limited noisy measurements of the system is inherently difficult. When posed as an optimization problem (for example, in the model predictive estimation approach described previously), one can expect that, in general, multiple local minima of such a nonconvex optimization problem will exist, many of which will be associated with state estimates that are in fact poor. These difficulties are exacerbated in the case of the estimation of near-wall turbulence by the fact that turbulence is a multiscale phenomenon (that is, it is characterized by energetic motions over a broad range of length scales and time scales that interact in a nonlinear fashion), with significant nonlinear chaotic dynamics evolving far from where sensors are located (that is, on the walls).

As illustrated, e.g., in Figure 1b of BL98 (that is, Bewley & Liu 1998), quantified by the "observation residual" in Table 1 of BL98, and discussed further in Part 1, even in the laminar case, at $k_x = 1$, $k_z = 0$ a significant number of the leading eigenmodes of the system are "center modes" with very little support near the walls, and are thus are nearly unobservable with wall-mounted sensors. As easily shown via similar plots in the turbulent case at the same and higher bulk Reynolds numbers, an even higher percentage of the leading eigenmodes of the linearized system are nearly unobservable (that is, have very little support near the walls) in the turbulent case, with the problem getting worse as the Reynolds number is increased. We thus see that the problem of estimating turbulence is fundamentally harder than the problem of estimating perturbations to a laminar flow even if the linear model of turbulence is considered as valid, simply due to the heightened presence of nearly unobservable modes.

In the present work we focus our attention primarily on getting an accurate state estimate fairly close to the walls, where the sensors are located. This is done with the idea in mind that, in the problem of turbulence control (which is our ultimate long-term objective in this effort, and the reason we are pursuing this line of investigation in the first place), it is the near-wall region only that, on average, turbulence "production" substantially exceeds "dissipation", as pointed out in Jimenez (1999). Thus, we proceed with the objective that, if we can

(*a*) estimate the fluctuations in the near-wall region with a sufficient degree of accuracy, then

(*b*) subdue these near-wall fluctuations with appropriate control feedback,

then we will have a net stabilizing effect on the turbulent motions in the entire flow system, even if we don't completely relaminarize the turbulent flow. It is thus, we hypothesize, unnecessary for us to estimate the precise motions of the flow far from the wall in order to realize our ultimate objective in this work. Flow-field fluctuations far from the wall, which will not be estimated accurately in this work, will (through nonlinear interactions) act as disturbances to excite continuously the state estimation error, while feedback from the sensors will be used to subdue continuously this error in the near-wall region.

1.5. *Comparison of the estimation and control problems applied to near-wall turbulence*

Another significant difference between the turbulence control and turbulence estimation problems is that, in the control problem, once (if) the control becomes effective, the system approaches a stationary state in which the linearization of the system is valid. In the estimation problem, on the other hand, even if the estimate at some time is quite accurate, the system is still moving on its chaotic attractor, so the linearization of the system about some mean state is not strictly valid. Thus, in this respect, it is seen that the turbulence estimation problem might be considered as being fundamentally harder than the turbulence control problem.

1.6. *Outline*

A brief review of the governing equations and some of the particular properties of the extended Kalman filter used in this work is given in §2. Section 3 collects and analyzes the relevant statistics from a direct numerical simulation of a turbulent channel flow at $Re_\tau = 100$ in order to build the estimator. The statistical data from §3 is then used in §4 to compute feedback gains (in Fourier space) and kernels (in physical space) for the estimator. The performance of the resulting estimator is evaluated via DNS in §5, and §6 presents some concluding remarks and suggestions for future improvements.

2. Governing equations

2.1. *State equation and identification of terms lumped into the "external forcing" f*

The system model considered in this work is the Navier–Stokes equation for the three velocity components $\{U, V, W\}$ and pressure P of an incompressible channel flow, written as a (nonlinear) perturbation about a base flow profile $\bar{u}(y)$ and bulk pressure variation $\bar{p}(x)$ such that, defining

$$\begin{pmatrix} U \\ V \\ W \\ P \end{pmatrix} = \begin{pmatrix} u \\ v \\ w \\ p \end{pmatrix} + \begin{pmatrix} \bar{u}(y) \\ 0 \\ 0 \\ \bar{p}(x) \end{pmatrix},$$

where $\{u, v, w, p\}$ denote the temporally-fluctuating components of the flow, we have

$$\frac{\partial u}{\partial t}+\bar{u}\frac{\partial u}{\partial x}+v\frac{\partial \bar{u}}{\partial y}=-\frac{\partial p}{\partial x}+\frac{1}{Re}\Delta u+n_1, \tag{2.1a}$$

$$\frac{\partial v}{\partial t}+\bar{u}\frac{\partial v}{\partial x}=-\frac{\partial p}{\partial y}+\frac{1}{Re}\Delta v+n_2, \tag{2.1b}$$

$$\frac{\partial w}{\partial t}+\bar{u}\frac{\partial w}{\partial x}=-\frac{\partial p}{\partial z}+\frac{1}{Re}\Delta w+n_3, \tag{2.1c}$$

$$\frac{\partial u}{\partial x}+\frac{\partial v}{\partial y}+\frac{\partial w}{\partial z}=0, \tag{2.2}$$

where

$$\begin{aligned} n_1 &= -u\frac{\partial u}{\partial x}-v\frac{\partial u}{\partial y}-w\frac{\partial u}{\partial z}-\frac{\partial \bar{p}}{\partial x}+\frac{1}{Re}\frac{\partial^2 \bar{u}}{\partial y^2}, \\ n_2 &= -u\frac{\partial v}{\partial x}-v\frac{\partial v}{\partial y}-w\frac{\partial v}{\partial z}, \\ n_3 &= -u\frac{\partial w}{\partial x}-v\frac{\partial w}{\partial y}-w\frac{\partial w}{\partial z}. \end{aligned} \tag{2.3}$$

By selecting the base flow profile $\bar{u}(y)$ as the mean flow,

$$\bar{u}(y)=\lim_{T\to\infty}\frac{1}{T\,L_x\,L_z}\int_0^T\int_0^{L_x}\int_0^{L_z} U\,\mathrm{d}z\,\mathrm{d}x\,\mathrm{d}t,$$

and selecting $\bar{p}(x)$ to account for the mean pressure gradient sustaining the flow. Note that we assume no-slip solid walls ($U = V = W = u = v = w = 0$ on $y = \pm 1$) and that periodic boundary conditions are applied in the x and z directions to the perturbations variables $\{u, v, w, p\}$. This facilitates decomposition of the perturbation problem (2.1) in the x and z directions using a Fourier series.

We now apply such a Fourier decomposition to (2.1), using hat subscripts ($\hat{}$) to denote the Fourier representation. The system may then be transformed to $\{\hat{v}, \hat{\eta}\}$ form in a straightforward fashion. Applying the Laplacian $\Delta = \partial^2/\partial y^2 - k^2$, where $k^2 = k_x^2 + k_z^2$, to the Fourier transform of (2.1b), substituting for $\Delta\hat{p}$ from the divergence of the Fourier transform of (2.1), and applying the Fourier transform of (2.2) gives the equation for $\hat{v}$. Subtracting ik_x times the Fourier transform of (2.1c) from ik_z times the Fourier transform (2.1a) gives the equation for $\hat{\eta} = ik_z\hat{u} - ik_x\hat{w}$. The result is the linear Orr–Sommerfeld/Squire equations at each wavenumber pair $\{k_x, k_z\}$ with an extra term accounting for the nonlinearity of the system

$$\begin{pmatrix}\Delta & 0\\ 0 & I\end{pmatrix}\begin{pmatrix}\dot{\hat{v}}\\ \dot{\hat{\eta}}\end{pmatrix}=\begin{pmatrix}\mathcal{L}_{OS} & 0\\ \mathcal{L}_C & \mathcal{L}_{SQ}\end{pmatrix}\begin{pmatrix}\hat{v}\\ \hat{\eta}\end{pmatrix}+\begin{pmatrix}ik_xD & k^2 & ik_zD\\ ik_z & 0 & -ik_x\end{pmatrix}\begin{pmatrix}\hat{n}_1\\ \hat{n}_2\\ \hat{n}_3\end{pmatrix}, \tag{2.4}$$

where

$$\begin{aligned} \mathcal{L}_{OS} &= -ik_x\bar{u}\Delta + ik_x\bar{u}'' + \Delta^2/Re, \\ \mathcal{L}_{SQ} &= -ik_x\bar{u} + \Delta/Re, \\ \mathcal{L}_C &= -ik_z\bar{u}', \end{aligned} \tag{2.5}$$

where $\{\hat{n}_1, \hat{n}_2, \hat{n}_3\}$ are given by the Fourier transform of (2.3), taking (from the Fourier transform of (2.2) and the definition of $\hat{\eta}$)

$$\hat{u}=\frac{i}{k^2}\Big(k_x\frac{\partial \hat{v}}{\partial y}-k_z\hat{\eta}\Big), \quad \hat{w}=\frac{i}{k^2}\Big(k_z\frac{\partial \hat{v}}{\partial y}+k_x\hat{\eta}\Big),$$

and where, with the walls located at $y = \pm 1$ and the velocities normalized such that the peak value of $\bar{u}(y)$ is 1, Re is the Reynolds number based on the centerline velocity and channel half-width. Note that, for $k_x = k_z = 0$, it follows immediately from the definition of this system that $\hat{v} = \hat{\omega} = 0$ for all y. For all other wavenumber pairs, multiplying (2.4) by the inverse of the matrix on its LHS, it is straightforward to write the governing equation as

$$\dot{\hat{q}} = A\hat{q} + B\hat{n}, \tag{2.6}$$

where

$$\hat{q} = \begin{pmatrix} \hat{v} \\ \hat{\eta} \end{pmatrix}, \quad \hat{n} = \begin{pmatrix} \hat{n}_1 \\ \hat{n}_2 \\ \hat{n}_3 \end{pmatrix}, \quad A = \begin{pmatrix} \Delta^{-1}\mathcal{L}_{OS} & 0 \\ \mathcal{L}_C & \mathcal{L}_{SQ} \end{pmatrix},$$

$$B = \begin{pmatrix} \Delta^{-1}\, ik_x D & \Delta^{-1}\, k^2 & \Delta^{-1}\, ik_z D \\ ik_z & 0 & -ik_x \end{pmatrix}.$$

Note that the terms in this expression depend on the wavenumber pair being considered, $\{k_x, k_z\}$, and that the state $\hat{q}$ is a continuous function of both the wall-normal coordinate y and the time coordinate t. Implementation of this equation in the computer requires discretization of this system in the wall-normal direction y and a discrete march in time t.

The present system may be linearized by replacing the exact expression for n by an appropriate stochastic model, which we will denote f, thereby obtaining the linear state-space model

$$\dot{\hat{q}} = A\hat{q} + B\hat{f}, \tag{2.7}$$

As the mean of n is everywhere zero, it is logical to select this stochastic model such that $E[f] = 0$, where the expectation operator $E[\cdot]$ is defined as the average over many many realizations of the stochastic quantity in brackets. The covariance of f will be modeled carefully based on the covariance of n observed in DNS, as discussed further in §2.3.

2.2. *Measurements*

The present work attempts to develop the best possible estimate of the state based on measurements of the flow on the walls. As discussed in Part 1, and in greater detail in Bewley & Protas (2004), the three measurements available on the walls are the distributions of the streamwise and spanwise wall skin friction and the wall pressure. This information is mathematically complete in the following sense: if this information is uncorrupted by noise and the external forcing on the system is known exactly, the entire state of the flow (even in the fully turbulent regime, and at any Reynolds number) is uniquely determined by these measurements at the wall in an arbitrarily small neighborhood of time t (*without* knowledge of the initial conditions). However, the actual identification of this state is quite another matter, as it reflects an ill-posed problem that is hyper-sensitive to all sorts of errors (e.g., modeling errors, measurement errors, numerical errors, series truncation errors, etc.). These errors are unavoidable, even in relatively "clean" numerical experiments. Thus, the problem of estimation may be viewed as a "smoothing problem", or an attempt to reconcile noisy measurements with an approximate dynamic model of the system.

In the present paper, we have chosen to transform the three measurements available on the walls (of streamwise and spanwise wall skin friction and wall pressure) to a slightly different form such that their effects on the estimation of the system (2.7), which is in $\{v, \eta\}$ form, is a bit more transparent. There is a bit of flexibility here; in the present work, we have chosen to define this transformed measurement vector r to contain scaled versions of the wall values of the wall-normal derivative of the wall-normal vorticity, η_y/Re, the second wall-normal derivative of the wall-normal velocity, v_{yy}/Re, and the pressure, p. Note that we can easily relate this transformed measurement vector to the raw measurements of $\tau_x = u_y/Re$, $\tau_z = w_y/Re$, and p on the walls, which might be available from a lab experiment, via the relation (in Fourier space)

$$\hat{r} \triangleq \begin{pmatrix} \frac{1}{Re}\hat{\eta}_y|_{wall} \\ \frac{1}{Re}\hat{v}_{yy}|_{wall} \\ \hat{p}|_{wall} \end{pmatrix} = \begin{pmatrix} ik_z & -ik_x & 0 \\ -ik_x & -ik_z & 0 \\ 0 & 0 & I \end{pmatrix} \begin{pmatrix} \hat{\tau}_x|_{wall} \\ \hat{\tau}_z|_{wall} \\ \hat{p}|_{wall} \end{pmatrix} \triangleq T \begin{pmatrix} \hat{\tau}_x|_{wall} \\ \hat{\tau}_z|_{wall} \\ \hat{p}|_{wall} \end{pmatrix}, \tag{2.8}$$

and we may relate the transformed measurement vector r to the state q via the simple relation

$$r = Cq + g \qquad \text{with} \quad C = \frac{1}{Re} \begin{pmatrix} 0 & \left.\frac{\partial}{\partial y}\right|_{wall} \\ \left.\frac{\partial^2}{\partial y^2}\right|_{wall} & 0 \\ \left.\frac{1}{k^2}\frac{\partial^3}{\partial y^3}\right|_{wall} & 0 \end{pmatrix}, \tag{2.9}$$

where g accounts for the measurement noise. The last row of the above relation is easily verified by taking $\partial/\partial x$ of the x-momentum equation plus $\partial/\partial z$ of the z-momentum equation, then applying continuity and the boundary conditions.

For the purpose of posing the present state estimation problem, the measurements are assumed to be corrupted by uncorrelated, zero-mean, white Gaussian noise processes, which are assembled into the vector $\hat{g}$ with an assumed covariance (in Fourier space) of

$$G = \begin{pmatrix} \alpha_\eta^2 & 0 & 0 \\ 0 & \alpha_v^2 & 0 \\ 0 & 0 & \alpha_p^2 \end{pmatrix}. \tag{2.10}$$

Note that such an assumption of uncorrelated, white (in space and time) noise is in fact a fairly realistic model for electrical noise in the sensors. Note also that, for a given covariance of f, which we shall define in the following section, the diagonal components of G effectively parameterize the balance between the two types of stochastic forcing in this problem, the measurement noise g and the stochastic forcing f, and thus reflect how much we "trust" our three types of measurements. If our trust in the measurements is increased (that is, if the diagonal components of G are reduced), then generally more feedback is applied by the resulting Kalman filter gains in order to correct the estimator more aggressively based on the information contained in the measurements.

A different parameterization for the noise covariance that might be of interest in a practical implementation, in which the physical sensors measure τ_x, τ_y, and p, is

$$G = T \begin{pmatrix} \alpha_{\tau_x}^2 & 0 & 0 \\ 0 & \alpha_{\tau_y}^2 & 0 \\ 0 & 0 & \alpha_p^2 \end{pmatrix} T^*, \tag{2.11}$$

where T is defined in (2.8) and the convenient relation given in (2.5) of Part 1 has been used to relate the covariance of the noise on the raw measurements to the present formulation. This parameterization should also be explored numerically in future work.

2.3. *Extracting the relevant statistics for state estimation from resolved simulations*

The performance of the estimator may be tuned by accurate parameterization of the relevant statistical properties of the forcing term f in the linearized state model, in addition to adjusting the parameterization of the statistical properties of the measurement noise

g. These statistics play an essential role in the computation of the Kalman filter feedback gains.

In the present work, we will assume that f is effectively uncorrelated from one time step to the next (that is, we assume that f is "white" in time) in order to simplify the design of the estimator. Subject to this central assumption, we proceed by developing an accurate model for the assumed spatial correlations of f. As the system under consideration is statistically homogeneous in the x and z directions, the covariance of the stochastic forcing f may be parameterized in physical space as

$$E[f_i(x,y,z,t)f_j(x+r_x,y',z+r_z,t')] = \delta(t-t')Q_{f_if_j}(y,y',r_x,r_z),$$

where $\delta(t)$ denotes the Dirac delta and where the covariance $Q_{f_if_j}$ is determined by calculating the statistics of the actual nonlinear forcing term n in a DNS,

$$Q_{f_if_j}(y,y',r_x,r_z) = \lim_{T\to\infty}\frac{1}{T\,L_x\,L_z}\int_0^T\int_0^{L_x}\int_0^{L_z} n_i(x,y,z)n_j(x+r_x,y',z+r_z)\,\mathrm{d}z\,\mathrm{d}x\,\mathrm{d}t. \tag{2.12}$$

As the system under consideration is statistically homogeneous, or "spatially invariant", in the x and z directions, it is more convenient to work with the Fourier transform of the two-point correlation $Q_{f_if_j}$ rather than working with $Q_{f_if_j}$ itself, as the calculation of $Q_{f_if_j}$ in physical space involves a convolution sum, which reduces to a simple multiplication in Fourier space. The Fourier transform of $Q_{f_if_j}$, which we identify as the spectral density function $R_{\hat{f}_i\hat{f}_j}$, is defined as

$$R_{\hat{f}_i\hat{f}_j}(y,y',k_x,k_z) = \frac{1}{4\pi}\int_{-L_x/2}^{L_x/2}\int_{-L_z/2}^{L_z/2} Q_{f_if_j}(y,y',r_x,r_z)\,\mathrm{e}^{-ik_xr_x-ik_zr_z}\,\mathrm{d}r_x\mathrm{d}r_z. \tag{2.13}$$

Note that, due to the statistical homogeneity of the system in x and z, the spectral density function $R_{\hat{f}_i\hat{f}_j}$ is a decoupled at each wavenumber pair $\{k_x,k_z\}$, and thus may be determined from the DNS according to

$$R_{\hat{f}_i\hat{f}_j}(y,y',k_x,k_z) = \lim_{T\to\infty}\frac{1}{T}\int_0^T \hat{n}_i(y,k_x,k_z)\hat{n}_j^*(y',k_x,k_z)\,\mathrm{d}t. \tag{2.14}$$

Certain symmetries may be applied to accelerate the convergence of the statistics determined from the DNS and to reduce the amount of covariance data that needs to be stored, which is in fact quite large. Since $Q_{f_if_j}$ is a real-valued function, $R_{\hat{f}_i\hat{f}_j}$ is Hermitian, so

$$R_{\hat{f}_i\hat{f}_j}(y,y',k_x,k_z) = R^*_{\hat{f}_i\hat{f}_j}(y,y',-k_x,-k_z). \tag{2.15}$$

By (2.14), it follows immediately that

$$R_{\hat{f}_i\hat{f}_j}(y,y',k_x,k_z) = R^*_{\hat{f}_j\hat{f}_i}(y',y,k_x,k_z). \tag{2.16}$$

Due to the up/down and left/right statistical symmetry in the flow, it also follows that

$$R_{\hat{f}_i\hat{f}_j}(y,y',k_x,k_z) = \pm R^*_{\hat{f}_i\hat{f}_j}(-y,-y',k_x,k_z), \tag{2.17a}$$

$$R_{\hat{f}_i\hat{f}_j}(y,y',k_x,k_z) = \pm R^*_{\hat{f}_i\hat{f}_j}(y,y',k_x,-k_z), \tag{2.17b}$$

$$R_{\hat{f}_1\hat{f}_3}(y,y',k_x,k_z) = R_{\hat{f}_2\hat{f}_3}(y,y',k_x,k_z) = 0, \tag{2.17c}$$

where, in (2.17a), the minus sign is used for the cases $\{i=2, j\neq 2\}$ and $\{i\neq 2, j=2\}$, and the positive sign is used for all other cases and, in (2.17b), the minus sign is used for the cases $\{i=3, j\neq 3\}$ and $\{i\neq 3, j=3\}$, and the positive sign is used for all other cases. The reader is referred to, e.g., Moin & Moser (1989) for similar computations. Finally, for later use, the individual components of the spectral density function $R_{\hat{f}\hat{f}}$ at each wavenumber pair $\{k_x, k_z\}$ are denoted by

$$R_{\hat{f}\hat{f}}(y, y', k_x, k_z) = \begin{pmatrix} R_{\hat{f}_1\hat{f}_1} & R_{\hat{f}_1\hat{f}_2} & R_{\hat{f}_1\hat{f}_3} \\ R_{\hat{f}_2\hat{f}_1} & R_{\hat{f}_2\hat{f}_2} & R_{\hat{f}_2\hat{f}_3} \\ R_{\hat{f}_3\hat{f}_1} & R_{\hat{f}_3\hat{f}_2} & R_{\hat{f}_3\hat{f}_3} \end{pmatrix}.$$

3. Statistics of the nonlinear term n

We now perform a direct numerical simulation of the nonlinear Navier–Stokes equation in a turbulent channel flow at $Re_\tau = 100$, gathering the statistics of the nonlinear term n identified in (2.3), which combines all those terms which will be supplanted by the stochastic forcing f in the linearized model (2.7) upon which the Kalman filter will be based.

Note that all DNS calculations performed in this work used the code of Bewley, Moin & Temam (2001). For the spatial discretization, this code uses dealiased pseudospectral techniques in the streamwise and spanwise directions and an energy-conserving second-order finite difference technique in the wall-normal direction. For the time march, the code uses a fractional step implementation of a hybrid second-order Crank–Nicolson / third-order Runge–Kutta–Wray method, as described in Aksevoll & Moin (1995). In all simulations, the overall pressure gradient is adjusted at each time step in order to maintain a constant mass flux in the flow, and a computational domain of size $4\pi \times 2 \times 4\pi/3$ in the $x \times y \times z$ directions is used. The resolution is $42 \times 64 \times 42$ Fourier, finite difference, Fourier modes (that is, $64 \times 64 \times 64$ dealiased collocation points). The numerical scheme used to discretize the Orr–Sommerfeld/Squire equations in this work is the spectral Differentiation Matrix Suite of Weideman & Reddy (2000); for details on how that scheme has been applied to our estimation problem, see Högberg *et al.* (2003*a*).

The covariance of the forcing term $n = (n_1, n_2, n_3)^T$ identified in (2.3) was sampled during a DNS calculation long enough to obtain statistical convergence. During the simulation, the full covariance matrices were computed at each wavenumber pair, creating a very large four-dimensional data set. The size of the covariance data is $N_x \times N_z \times N_y^2$ for each correlation component of the forcing vector (before exploiting any symmetries), where N_x, N_y, and N_z denote the resolution in the corresponding directions. As resolution requirements of turbulence simulations increase quickly with increasing Reynolds number, at higher Reynolds numbers it soon becomes necessary to represent only the most significant components of these correlations via some sort of reduced-order modeling technique, such as Proper Orthogonal Decomposition via the "snapshot" method. The symmetries mentioned in §2.3 were then applied in post processing to improve the statistical convergence. These statistics are subsequently used in §4, where the optimal estimation feedback gains are computed. In §5, the feedback gains so determined are used in order to estimate a fully turbulent flow based on wall measurements alone. Both Kalman filters and extended Kalman filters are investigated.

In Figure 1 the magnitude of the spectral density function at four representative wavenumber pairs $\{k_x, k_z\}$ are plotted. As seen in the figure (plotted along the main diagonal), the variance of the forcing terms is stronger in the high shear regions near the walls, as expected. Note also that there is a pronounced cross-correlation between f_1 and f_2, accounting for the Reynolds stresses in the flow, with the other cross-correlations converging towards zero as the statistical basis is increased. Figure 3a shows the corresponding variation of the maximum magnitude of the spectral density function as a

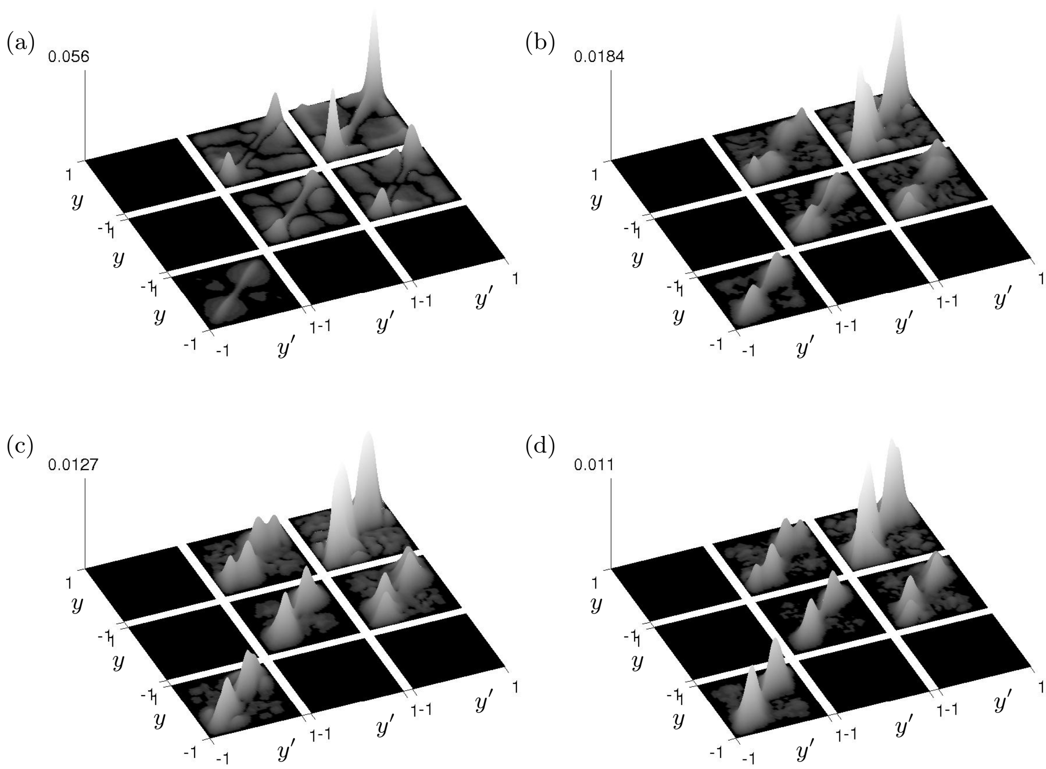

FIGURE 1. The magnitude of the spectral density function $R_{\hat{f}\hat{f}}(y, y', k_x, k_z)$ of $\hat{f}$, computed from the DNS of a turbulent channel flow at $Re_\tau = 100$, at wavenumber pairs $\{k_x, k_z\}$ of (a) $\{1.0, 3.0\}$, (b) $\{3.0, 1.5\}$, (c) $\{0.0, 1.5\}$, and (d) $\{4.0, 4.5\}$. The nine "squares" correspond to the correlation between the various components of the forcing vector; from furthest to the viewer to closest to the viewer, the squares correspond to the $\hat{f}_1$, $\hat{f}_2$, and $\hat{f}_3$ components on each axis. The width of each side of each square represents the width of the channel, $[-1, 1]$. The variance is plotted along the diagonal of each square.

function of the wavenumbers k_x and k_z. As expected, the stochastic forcing is stronger for lower wavenumber pairs.

Figure 2, a corresponding plot of the magnitude of the spectral density function of the stochastic forcing model defined in Part 1 is given. Note that the shape of this covariance model is invariant with $\{k_x, k_z\}$, it is only the overall magnitude of this covariance model that varies with $\{k_x, k_z\}$, in contrast with the covariance data determined from the DNS data, as reported in Figure 1. Figure 3b shows the corresponding variation of the maximum magnitude of the spectral density function as a function of the wavenumbers k_x and k_z.

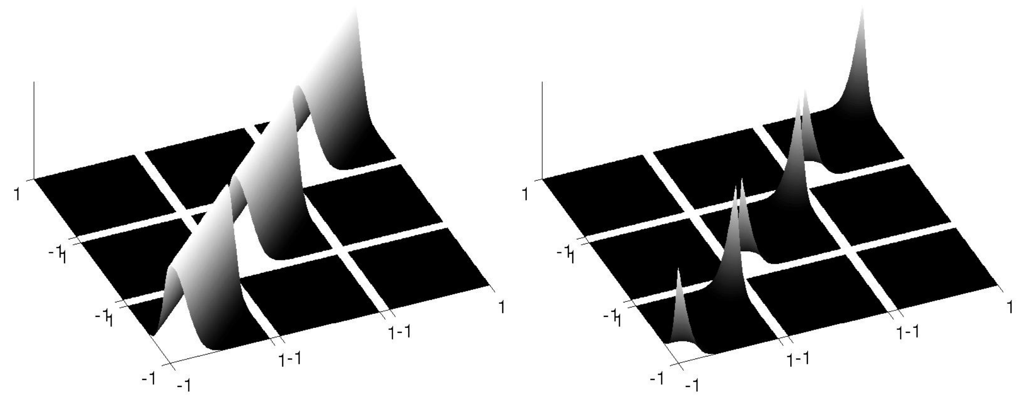

FIGURE 2. The magnitude of the spectral density function $R_{\hat{f}\hat{f}}(y, y', k_x, k_z)$ of $\hat{f}$, as parameterized in the laminar model proposed in Part 1 of this study, taking $p = 0$ (left) and $p = 3$ (right); see Figure 1 for further explanation of the plot.

(a) (b)

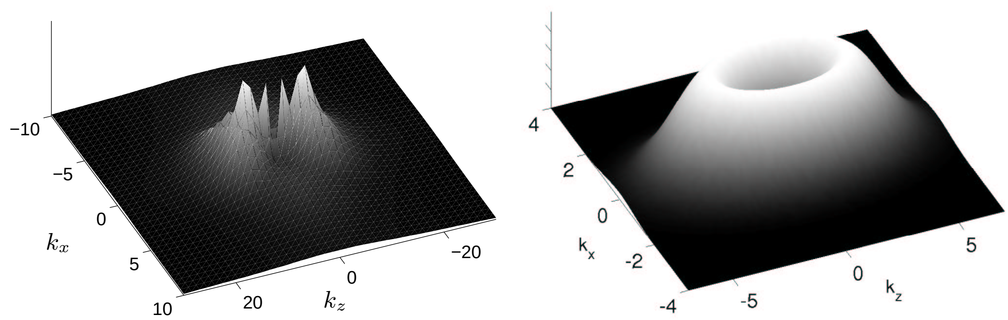

FIGURE 3. The variation of the maximum amplitude of the spectral density function as a function of the wavenumbers k_x and k_z for the DNS data (left) and the statistical model of Part 1 (right).

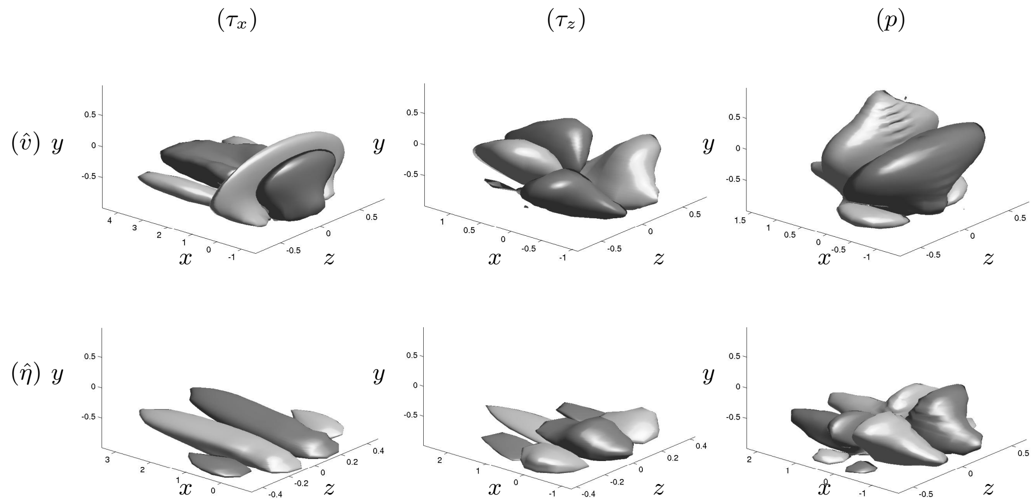

FIGURE 4. Isosurfaces of the physical space convolution kernels determined for $Re_\tau = 100$ turbulent channel flow based on the statistics of the neglected terms in the linearized model, as determined by DNS and plotted in Figures 1 and 3a. Shown are the steady-state convolution kernels relating the (*left*) τ_x, (*center*) τ_z, and (*right*) p measurements at the point $\{x = 0,\ y = -1,\ z = 0\}$ on the wall to the estimator forcing on the interior of the domain for the evolution equation for the estimate of (*top*) v and (*bottom*) η. Visualized are positive (dark) and negative (light) isosurfaces with isovalues of $\pm 5\%$ of the maximum amplitude for each kernel illustrated. Note that these kernels are substantially different in shape with those used in the laminar case, as reported in Figure 12 of Part 1; in particular, note that they are generally more focused in the region adjacent to the lower wall, likely as consequence of the fuller mean velocity profile about which the system is linearized in the turbulent case.

4. Estimator gains and the corresponding physical-space kernels

In previous studies the covariance Q has been modeled with a spatially uncorrelated stochastic forcing, as for example in Högberg *et al.* (2003*a*). With that model it proved to be impossible to compute well resolved estimation gains for more than one measurement (of η_y). In contrast, the present study models the stochastic forcing Q based on R, as defined in (2.13) and determined from a DNS database. Basing the stochastic model on the turbulent statistics makes it possible to render well resolved gains for all three measurements, η_y, v_{yy}, and p. In Part 1 it is shown that well resolved estimation gains for the three measurements τ_x, τ_z, and p, can be achieved by designing the covariance model to be more physically realistic. The definition and solution procedure for the state estimation problem in order to solve for the Kalman filter gains in the estimator in the present work is identical to that described in Part 1 of this study, to which the reader is referred for details.

Figure 4 illustrates isosurfaces of the physical-space convolution kernels based on the statistics of the neglected terms in the linearized model, as determined from DNS. (Note, however, that these gains are transformed to gains based on η_y, v_{yy}, and p in the estimator simulations presented in §5). Note that these kernels depicted in Figure 4 are substantially different in shape from those used in the laminar case, as reported in Figure 12 of Part 1; in particular, note that they are generally more focused in the region adjacent to the lower wall, likely as consequence of the fuller mean velocity profile about which the system is linearized in the turbulent case.

The sensor noise, described in §2.2, is a natural "knob" to tune the strength of the individual measurements as well as their relative strength. Note that the sensor noise level

Case	α_η	α_v	α_p	Q	$J^{1/2}$
1	0.1200	–	–	I	52
2	0.0037	–	–	$R_{\hat{f}_1\hat{f}_1}$	52
3	0.0030	0.0030	0.0075	$R_{\hat{f}\hat{f}}$	53

TABLE 1. The estimation simulations. For the cases when using one measurement, only the corresponding α is relevant since the other measurements are excluded from the C-matrix.

will also affect the shape of the estimation gains. In an attempt to make a reasonably fair comparison between the different stochastic models we consider the following measure

$$J = \int_{-1}^{1}\int_{0}^{L_x}\int_{0}^{L_z} L_{\eta_y}^2 \,\mathrm{d}x\,\mathrm{d}y\,\mathrm{d}z,$$

i.e., the integral in all three spatial directions of the gain corresponding to the η_y measurement, L_{η_y}. Three cases were studied, as shown in Table 1. In all three cases, the relevant α parameters were tuned so that the integrated strength J is approximately equal. Each measurement captures different features of the flow field and by this study we want to characterize what additional information we get when the two new measurements are added and the covariance of the system accurately modeled, rather than investigating how the strength is distributed over estimator gains and how that affects the estimation process. Note that the resulting strength of the gains require no adjustment of the time step in the extended Kalman filter DNS to run properly.

5. Estimator performance

5.1. *Estimator algorithm*

In order to quantify the performance of the Kalman filter developed in this work, we run two direct numerical simulations in parallel. One simulation represents the "real" flow, where the initial condition is a fully developed turbulent flow field. The other simulation is the estimated flow field. The real flow is modeled by the the Navier–Stokes equations. In the estimator simulations we have tested both the Kalman filters (with the state model being the linearized Navier–Stokes equation) and extended Kalman filter (with the state model being the full nonlinear Navier–Stokes equation). The initial condition for the estimator simulations is a turbulent mean flow profile with all fluctuating velocity components set to zero. In both estimator simulations the volume forcing v, defined in §1.2, is added. The additional forcing is based on wall measurements and the precomputed estimation gains. For the Kalman filter simulations we enforce the turbulent mean flow profile that we linearized about and allow no nonlinear interactions to take place in the estimator, by scaling down the fluctuations to a sufficiently small amplitude to suppress nonlinear interactions (This method was necessary with the present version of our DNS code to enforce a linear simulation).

To evaluate the performance of the Kalman and extended Kalman filters the correlation between the actual and estimated flow is computed throughout the wall-normal extent of the domain at each instant of time,

$$\mathrm{corr}_y(s,\hat{s}) = \frac{\int_0^{L_x}\int_0^{L_z} s\hat{s}\,\mathrm{d}x\,\mathrm{d}z}{\left(\int_0^{L_x}\int_0^{L_z} s^2\,\mathrm{d}x\,\mathrm{d}z\right)^{1/2}\left(\int_0^{L_x}\int_0^{L_z} \hat{s}^2\,\mathrm{d}x\,\mathrm{d}z\right)^{1/2}}, \tag{5.1}$$

where s and $\hat{s}$ represent either u, v, w, or p from the actual and estimated flow, respectively. A correlation of one means perfect correlation whereas zero correlation zero means no correlation at all.

Another useful quantity to study is the error between the actual and estimated flow state, defined as

$$\text{errn}_y(s,\hat{s}) = \frac{\left(\int_0^{L_x}\int_0^{L_z}(\hat{s}-s)^2\,\mathrm{d}x\mathrm{d}z\right)^{1/2}}{\left(\int_0^{L_x}\int_0^{L_z}s^2\,\mathrm{d}x\mathrm{d}z\right)^{1/2}}. \tag{5.2}$$

The error (5.2) ranges from zero, which means no error between the real and estimated flow fields, and infinity. However the most pertinent quantity to measure is the total energy of the error between the real and estimated flow fields defined as

$$\text{errn}_y^{\text{tot}}(q,\hat{q}) = \frac{\left(\int_0^{L_x}\int_0^{L_z}(\hat{q}-q)^*\mathcal{Q}(\hat{q}-q)\,\mathrm{d}x\mathrm{d}z\right)^{1/2}}{\left(\int_0^{L_x}\int_0^{L_z}q^*\mathcal{Q}q\,\mathrm{d}x\mathrm{d}z\right)^{1/2}}. \tag{5.3}$$

since this is the quantity that we, in an average sense, are minimizing for in the construction of the optimal estimation gains. Operator $\mathcal{Q}$ represent the energy inner-product in (v,η) coordinates (see e.g. Schmid & Henningson 2001).

5.2. *One measurement — two stochastic models*

To compare the gains based on a spatially uncorrelated stochastic model with the estimation gains based on the stochastic model suggested in this study, we first compare the performance of the estimator using only the η_y measurement. This is because we only obtained a well-resolved estimation gain for the η_y measurement when using the spatially uncorrelated stochastic model.

The correlation between the real and estimated flow, for one measurement, is depicted in Figure 5 and Figure 6 for the Kalman and extended Kalman filters respectively. The dashed lines represent the stochastic model developed in this work whereas the dash-dotted lines represent the spatially uncorrelated stochastic model. The correlation for the u-component is almost the same close to the wall for the two filters but there is an increasing difference both for the Kalman and extended Kalman filter as the wall distance increases. For v, w, and p the difference is larger. In Figure 7 and Figure 8 we can see similar trends for all the primitive variables and for both the Kalman and extended Kalman filter. We anticipated a more pronounced difference between the two stochastic models but apparently the importance of the stochastic model is not crucial for the performance of the η_y measurement, alone.

The correlation for the u-velocity component is close to one (perfect correlation) while the other components show only weak correlation. This is due to the fact that the streamwise disturbance velocity contains more energy than the other components and that with only the η_y measurement we are missing important information about the flow behavior.

For both the estimators with the present η_y gains and the estimator with gains based on the previous stochastic model, the correlation and error for the u-component, decay quickly once we get beyond $y^+ \approx 8$ and in the center region of the channel both the error and correlation measures are performing poorly. v, w, and p are clearly not estimated very well with only the η_y measurement. p is constantly on a low level whereas v and w experiences a similar decay as u once the wall distance increases.

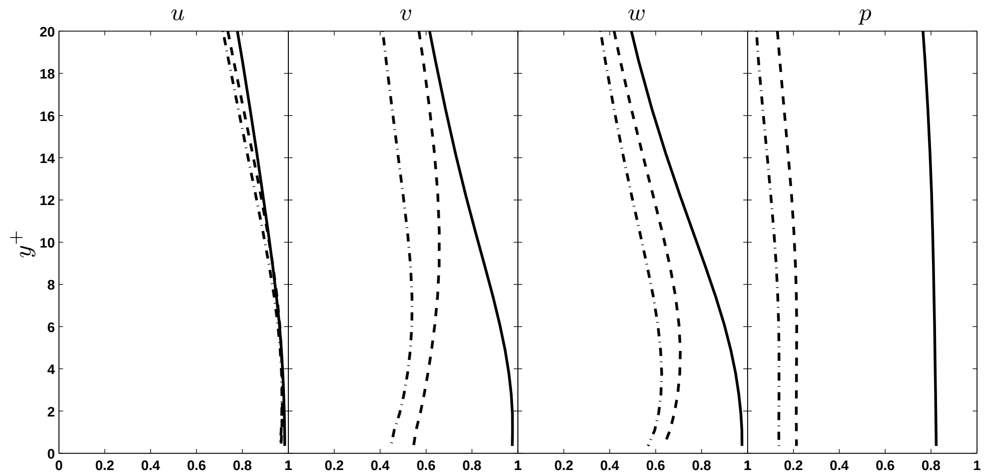

FIGURE 5. The figure shows $\mathrm{corr}_y(s, \hat{s})$ for $s = u$, $s = v$, $s = w$, and p obtained using Kalman filter. The solid line denotes estimation using all three measurements and noise statistics as discussed in §3. The dashed line denotes the estimator performance using only the η_y measurement. The dash-dotted line is obtained using the spatially uncorrelated stochastic model for noise statistics.

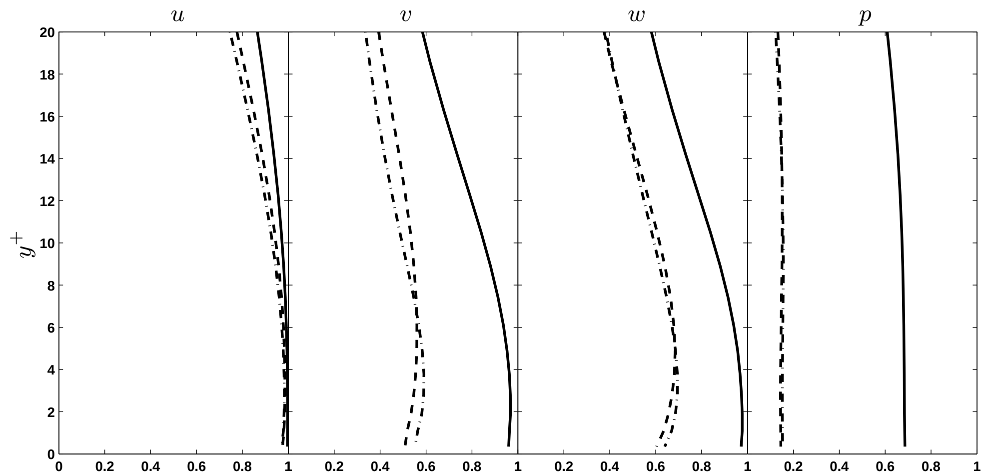

FIGURE 6. The figure shows $\mathrm{corr}_y(s, \hat{s})$ for $s = u$, $s = v$, $s = w$, and p obtained using extended Kalman filter. For a definition of the curves see, Figure 5.

5.3. *Three measurements — one stochastic model*

The performance of all three measurements combined, with the relative weighting presented in table 1, are shown as solid lines in Figure 5 – 8. In these figures it is clearly seen that the correlation and error between the real and estimated flow for all quantities v, w, and p is greatly improved when the additional measurements are included. The strongest improvement appears for the pressure, due to the addition of a pressure measurement.

In Figure 9 the total estimation error, averaged in time, is plotted as a function of wall-normal distance . The thin lines show the Kalman filter results and the thick lines the corresponding extended Kalman filter results. The improved estimation possibilities with the stochastic model presented in this study over a spatially uncorrelated one is clearly seen in Figure 9. The improvement is more pronounced closer to the wall.

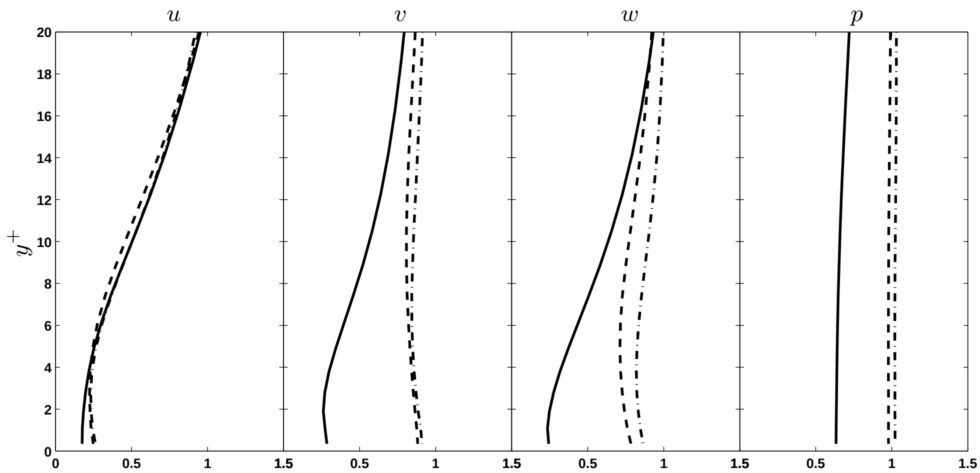

FIGURE 7. The relative estimation error $\mathrm{errn}_y(s, \hat{s})$, defined as in equation (5.2) plotted for the Kalman filter. The solid line denotes estimation performed with all three measurements and gains based on turbulence statistics. The dashed line denotes the estimator performance using only the η_y measurement. The dash-dotted line is the correlation when using the spatially uncorrelated stochastic model.

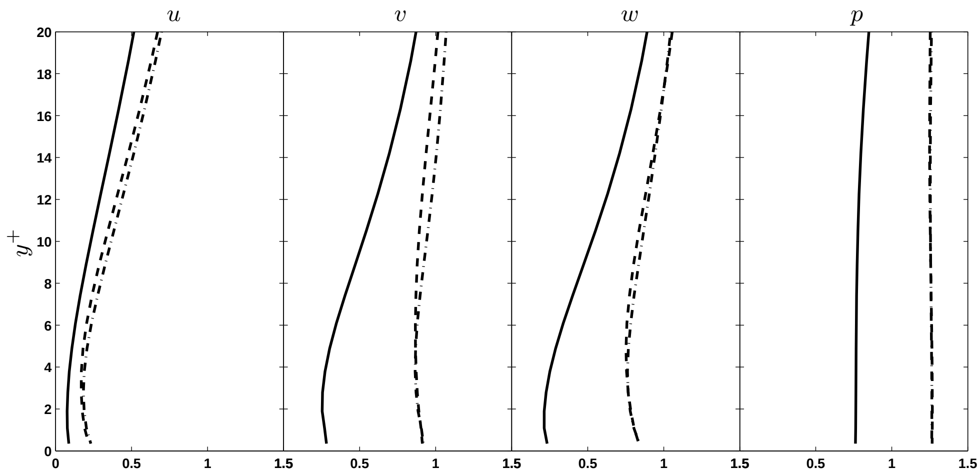

FIGURE 8. The relative estimation error, defined as in equation (5.2), plotted for the extended Kalman filter. For a definition of the curves see, Figure 7.

For both the estimator with the present η_y gains and the estimator with gains based on the previous stochastic model, the correlation and error for the u, v, and w quantities drop off quickly once we get beyond $y^+ \approx 10$ and in the center region of channel both the error and correlation measures are performing poorly.

The total energy of the estimation error displays a transient phase when the two simulations are started. This transient is depicted in Figure 10 for the Kalman filter simulation. Closer to the wall the transient is stronger and the error reaches a lower level than further into the flow domain. The transient is due to the fact that the estimated flow is initiated with only a turbulent mean flow profile.

The performance of our estimator can be compared with the result reported in Bewley & Protas (2004), where a turbulent channel flow at $Re_\tau = 180$ is estimated from limited

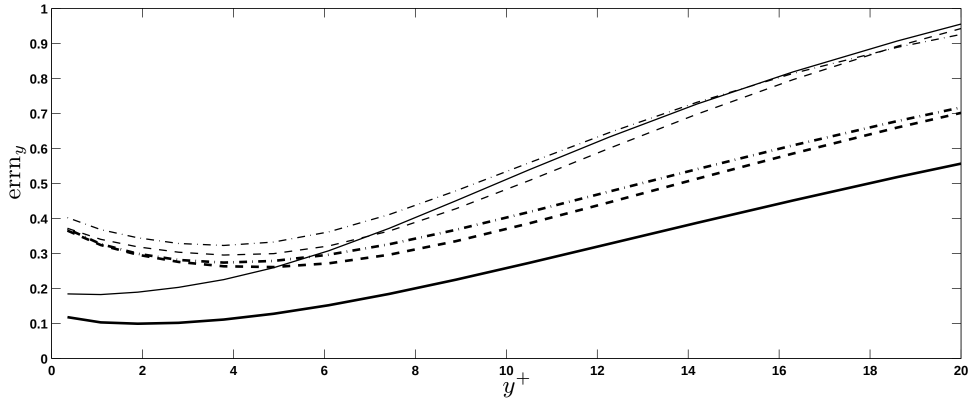

FIGURE 9. The total energy of the estimation error is shown as a function of the wall-normal distance. The solid line denotes the error when all three measurements are applied in the estimator. The dashed and dash-dotted lines represent the estimator performance when using only the η_y measurement with the stochastic model based on turbulence statistics and the spatially uncorrelated stochastic model respectively. The thick lines show the extended Kalman filter and the thin lines the Kalman filter data.

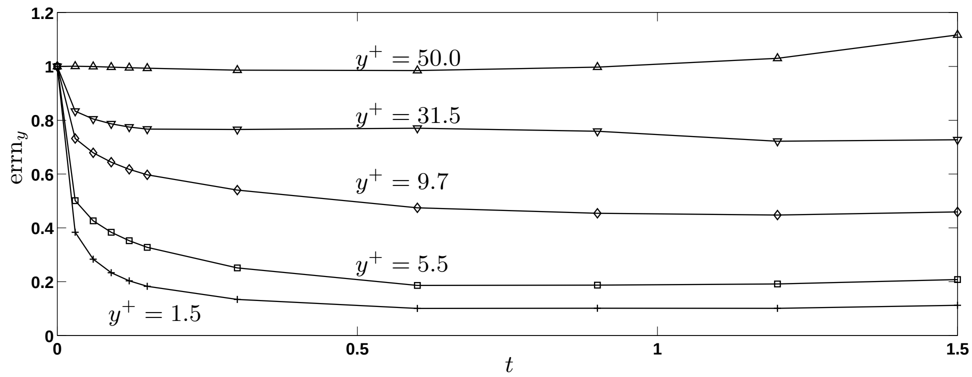

FIGURE 10. The transient behavior of the total error energy at $y^+ = 1.5$, $y^+ = 5.5$, $y^+ = 9.7$, $y^+ = 31.5$, and along the channel centerline for case 3 in table 1. All three measurements are used together with the Kalman filter.

measurements as discussed in §1.1. The adjoint method is computationally demanding but gives the optimal estimate of the flow at a certain time with respect to the chosen objective function. Since the present results are computed for a lower Reynolds number we can compare only qualitatively the performances. The adjoint simulation results show the same overall trends both correlation as well as in terms of estimation error.

In Figure 11, an instantaneous plot of the v velocity component is shown at $y^+ = 9.7$ for the flow field and the two different filters (based on three measurements). Similar structures are present in all three cases. At some instants of time the Kalman filter even has a better match compared to the extended Kalman filter with the real flow but Figure 11 gives an idea of the general trend. The Kalman filter performance also deteriorates more quickly as the wall normal distance is increased and the structures are slightly weaker than in the extended Kalman filter.

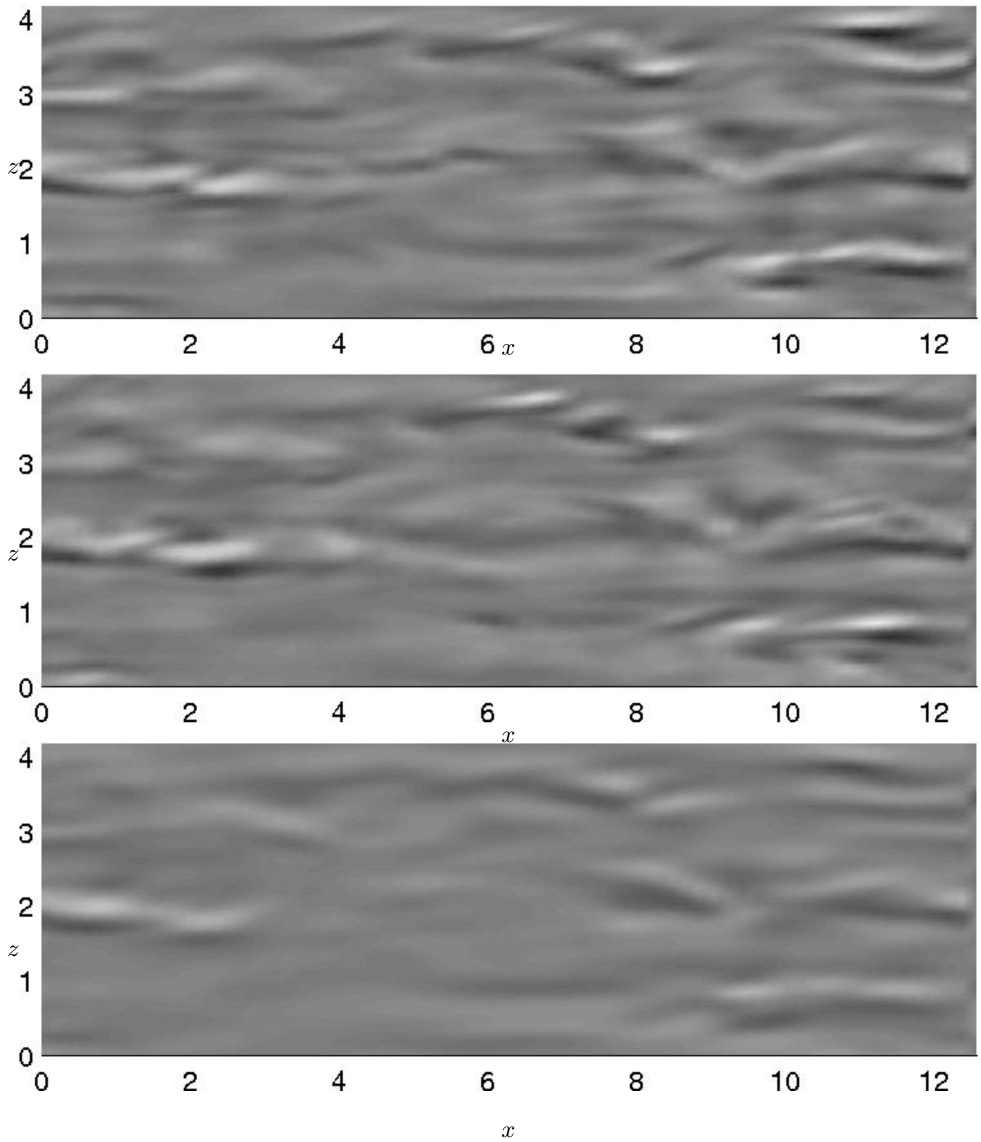

FIGURE 11. Wall-normal velocity component v plotted at $y^+ = 9.7$ at an instant in time. In the top figure the flow velocity itself is plotted. The middle plot shows the velocity field reproduced by the extended Kalman filter, and the bottom plot shows the velocity field reproduced by the Kalman filter. The contour levels range from -1 to 1, where black and white represent the lower and upper bound respectively.

6. Summary and conclusions

A key step in the framing the Kalman filter problem is the accurate statistical description of the system dynamics not fully described by the estimator model. The present paper has shown that, by determining the appropriate second-order statistical information in a full nonlinear DNS of the channel flow system, then incorporating this statistical information in the computation of the estimator feedback gains, an effective estimator may be built based on all three measurements available at the wall. For a given feedback amplitude, this estimator provides a better correlation between the real turbulent flow and the estimate thereof than the corresponding estimators considered for this problem in previous work. Significant improvements are obtained, as compared with estimators based on spatially uncorrelated stochastic models, in terms of both the maximum correlation as well as how far into the channel an accurate correlation extends. Also, the estimation gains may be transformed to physical space to obtain well-resolved convolution kernels that eventually decay exponentially with distance from the origin, thereby, ultimately, facilitating decentralized implementation.

In Part 1 of this study, Hœpffner *et al.* (2004), the estimation of a perturbed laminar flow was investigated, and it was shown that an artificial, but physically reasonable, Gaussian distribution model for the spectral density function was adequate to obtained effective, well-behaved estimation feedback kernels for the problem of estimating the perturbed laminar flow. That result, together with the result from the present study for the problem of estimating turbulence, indicate that the choice of the disturbance model is quite significant in the estimation problem, but a highly accurate statistical model is actually not essential.

As expected, the (nonlinear) extended Kalman filter was found to outperform a (linear) Kalman filter on this nonlinear estimation problem. The estimated state in the Kalman filter deteriorates more rapidly with the distance from the wall. The extended Kalman filter captures better the structures further into the domain, both in magnitude and phase. In terms of both correlation and estimation error, we also observed an approximate correspondence with the performance of the present extended Kalman filter with the adjoint-based estimation procedure reported in Bewley & Protas (2004). The adjoint-based approach is vastly more expensive computationally, and, at least in theory, can account for the nonlinear dynamics of the system more accurately, so this correspondence reflects favorably on the performance of the present extended Kalman filter.

The admittedly artificial assumption of the external disturbance forcing $\tilde{f}$ being "white" in time may be relaxed in future work, "coloring" the noise with the time dynamics of f, by performing a spectral factorization of f in both space and time and augmenting the estimator model to account for the dominant time dynamics in $\tilde{f}$. This approach, while in theory tractable for this problem, involves estimators of substantially higher dimension than the present (which is already large), and might facilitate substantial performance improvements. Development of this approach is thus deferred for the time being as a promising area for future work on this problem.

Acknowledgement

The authors sincerely acknowledge the funding provided by the Swedish research council (VR), the Swedish defence research agency (FOI), and the Dynamics and Control directorate of the Air Force Office of Scientific Research (AFOSR) in support of this work.

REFERENCES

Aksevoll, K. & Moin, P. 1995 Large eddy simulations of turbulent confined coannular jets and turbulent flow over a backward facing step. Technical Report Report TF-63. Thermosciences Division, Dept. of Mech. Eng., Stanford University.

Anderson, B. & Moore, J. 1979 *Optimal filtering*. Prentice-Hall.

Balakrishnan, A. V. 1976 *Applied functional analysis*. Springer.

Bamieh, B. 1997 The structure of the optimal controller of spatially invariant ditributed parameter systems. In *Proc. 36th IEEE Conf. on Decision and Control*.

Bewley, T. R. 2001 Flow control: new challenges for a new renaissance. *Progress in Aerospace Sciences* **37**, 21–58.

Bewley, T. R., Moin, P. & Temam, R. 2001 DNS-based predictive control of turbulence: an optimal benchmark for feedback algorithms. *J. Fluid Mech.* **447**, 179–225.

Bewley, T. R. & Protas, B. 2004 Skin friction and pressure: the "footprints" of turbulence. *Physica D* **196**, 28–44.

Farrell, B. F. & Ioannou, P. J. 1996 Turbulence suppression by active control. *Phys. Fluids* **8**, 1257–1268.

Hœpffner, J., Chevalier, M., Bewley, T. R. & Henningson, D. S. 2004 State estimation in wall-bounded flow systems, Part 1. Laminar flows. *J. Fluid Mech.* Submitted.

Högberg, M., Bewley, T. R. & Henningson, D. S. 2003*a* Linear feedback control and estimation of transition in plane channel flow. *J. Fluid Mech.* **481**, 149–175.

Högberg, M., Bewley, T. R. & Henningson, D. S. 2003*b* Relaminarization of $Re_\tau = 100$ turbulence using gain scheduling and linear state-feedback control. *Phys. Fluids* **15**, 3572–3575.

Jimenez, J. 1999 The physics of wall turbulence. *Physica A* **263**, 252–262.

Jovanović, M. R. & Bamieh, B. 2001 Modelling flow statistics using the linearized Navier–Stokes equations. In *Proceedings of the 40th IEEE Conference on Decision and Control*, pp. 4944–4949. Orlando, FL.

Kim, J. & Lim, J. 2000 A linear process in wall-bounded turbulent shear flows. *Phys. Fluids* **12** (8), 1885–1888.

Lewis, F. L. & Syrmos, V. L. 1995 *Optimal control*. Wiley-Interscience.

Moin, P. & Moser, R. D. 1989 Characteristic-eddy decomposition of turbulence in a channel. *J. Fluid Mech.* **200**, 471–509.

Schmid, P. J. & Henningson, D. S. 2001 *Stability and transition in shear flows*. Springer.

Weideman, J. A. & Reddy, S. 2000 A matlab Differentiation Matrix Suite. *ACM Transaction of Mathematical Software* **26** (4), 465–519.